HHS Public Access

Author manuscript

Nat Metab. Author manuscript; available in PMC 2019 September 18.

Published in final edited form as:

Nat Metab. 2019 February ; 1(2): 251–260. doi:10.1038/s42255-018-0020-9.

The hepatokine Tsukushi gates energy expenditure via brown fat sympathetic innervation

Qiuyu Wang[1], **Vishal P. Sharma**[1], **Hong Shen**[2], **Yuanyuan Xiao**[1], **Qi Zhu**[3], **Xuelian Xiong**[1], **Liang Guo**[1], **Lin Jiang**[2], **Kunimasa Ohta**[4], **Siming Li**[1], **Haifei Shi**[3], **Liangyou Rui**[2], **Jiandie D. Lin**[1,*]

[1]Life Sciences Institute and Department of Cell & Developmental Biology, University of Michigan Medical Center, Ann Arbor, MI 48109

[2]Department of Molecular & Integrated Physiology, University of Michigan Medical Center, Ann Arbor, MI 48109

[3]Physiology and Neuroscience, Department of Biology, Miami University, OH 45056

[4]Department of Developmental Neurobiology, Graduate School of Life Sciences, Kumamoto University, Kumamoto, Japan

Abstract

Thermogenesis is an important contributor to whole body energy expenditure and metabolic homeostasis. Although circulating factors that promote energy expenditure are known, endocrine molecules that suppress energy expenditure have remained largely elusive. Here we show that Tsukushi (TSK) is a liver-enriched secreted factor that is highly inducible in response to increased energy expenditure. Hepatic Tsk expression and plasma TSK levels are elevated in obesity. TSK deficiency increases sympathetic innervation and norepinephrine release in adipose tissue, leading to enhanced adrenergic signaling and thermogenesis, attenuation of brown fat whitening and protection from diet-induced obesity in mice. Our work reveals TSK as part of a negative feedback mechanism that gates thermogenic energy expenditure and highlights TSK as a potential target for therapeutic intervention in metabolic disease.

Endocrine hormones released by peripheral tissues, such as adipose tissue, skeletal muscle and the liver, play an important role in metabolic crosstalk and homeostasis [1-4]. The adipose tissue hormone leptin acts on the central nervous system to suppress food intake and promote energy expenditure [5,6]. Defects in the neuroendocrine circuitry that mediates leptin action have been linked to obesity and metabolic disorders. Fibroblast Growth Factor 21 (FGF21) is a hepatokine that exerts pleiotropic metabolic effects, including the stimulation

*Corresponding author: Jiandie Lin, Ph.D., 5437 Life Sciences Institute, University of Michigan, 210 Washtenaw Avenue, Ann Arbor, MI 48109, jdlin@umich.edu, Office: (734) 615-3512, Fax: (734) 615-0495.

Author contributions

J.D.L. and Q.W. conceived the project and designed research. Q.W., V.P.S., H. Shen, Y.X., Q.Z., X.X., L.G., H. Shi, S.L., L.R., and L.J. performed the experiments and analyzed data. K.O. provided Tsk knockout mouse strain. J.D.L. and Q.W. wrote the manuscript.

Conflict of interest statement

The authors declare no conflict of interest.

of brown and beige fat thermogenesis [2,7,8]. These observations underscore the importance of hormonal signals that promote energy expenditure in the maintenance of systemic energy and nutrient balance. In contrast, whether there exist endocrine factors that serve as a negative feedback signal to restrict energy expenditure in the hypermetabolic states remains essentially unknown. While Ghrelin is known to act as a hunger hormone that stimulates appetite and feeding and represses energy expenditure, inactivation of Ghrelin and its receptor produced modest effects on whole body energy balance [9]. We postulated that other hormonal signals likely constitute a critical feedback regulatory arm of energy homeostasis that puts a brake on energy expenditure to maintain systemic energy balance.

Adipose tissue is central for nutrient and energy homeostasis. White adipose tissue (WAT) stores energy, releases endocrine factors, and undergoes drastic structural and functional remodeling in obesity [10-13]. Brown adipose tissue (BAT) contains abundant mitochondria and generates heat via uncoupled respiration mediated by uncoupling protein 1 (UCP1) [14-17]. Recent studies have implicated UCP1-independent mechanisms in driving thermogenesis in beige fat [18-20]. Beyond thermogenesis, brown and beige fat releases endocrine factors such as Neuregulin 4 (Nrg4) to regulate hepatic lipid metabolism and preserve hepatocyte health under metabolic stress conditions [21-23]. Genetic ablation of brown fat renders mice cold-sensitive and exacerbates diet-induced weight gain [24], whereas activation of BAT thermogenesis has been linked to increased energy expenditure, reduced adiposity, and lower plasma lipid levels [25-27]. Brown fat thermogenesis is stimulated in response to cold exposure through increased adrenergic signaling to the depot and local bioactive thyroid hormone production, leading to activation of the thermogenic gene program and fuel oxidation [15].

In this study, we performed liver secretome analysis and identified Tsukushi (TSK) as an inducible hepatokine that responds to increased energy expenditure. TSK acts as a hormonal checkpoint that suppresses adipose tissue sympathetic innervation, adrenergic action and thermogenesis. Our work illustrates the existence of powerful endocrine hormones that dampen energy expenditure and reveals an intriguing opportunity for targeting TSK to restore energy balance and improve metabolic parameters in obesity.

Results

TSK is a hepatokine inducible in response to energy expenditure

We postulated that the liver provides a source of putative regulators of energy balance for several reasons. The liver itself is highly responsive to nutritional, hormonal and neural cues by integrating a wide array of nutrient and energy sensing pathways. Hepatocytes undergo drastic reprogramming of the release of secreted factors, such as FGF21, under different physiological and stress conditions [2]. We took an unbiased bioinformatic approach to first identify secreted factors that exhibit enriched or restricted expression in the liver. We examined mRNA expression profile of approximately 1,384 genes annotated to encode secreted proteins in a panel of 12 mouse tissues, including different brain regions and peripheral tissues (GSE54650). Clustering analysis revealed a highly restricted pattern of tissue distribution for this secretome gene set, illustrating the remarkable specificity and diversity of protein secretion by different tissues (Fig. 1a and Supplementary Table 1). As

expected, leptin and Nrg4 were among the top secreted factor hits in WAT and BAT, respectively. We identified a cluster of 129 genes exhibiting over 5-fold enriched expression in mouse liver compared to the averaged expression values from other tissues (red box, Fig. 1a and Supplementary Table 2). As expected, many of these liver-enriched secreted factors have known biological functions in lipoprotein metabolism, blood clotting, complement activation and endocrine signaling. The latter included Lipocalin 13 and Fetuin B, two liver-derived endocrine factors implicated in the regulation of glucose and lipid metabolism [28,29]. As the tissue panel was obtained from healthy mice, it is possible that our analysis may not include secretome genes specifically induced under pathological conditions.

We hypothesized that the putative inhibitory regulators of energy expenditure may be induced in hypermetabolic states to restore energy balance by serving as a feedback signal. As such, we next examined regulation of the liver secretome genes in hypermetabolic mice induced by chronic triiodothyronine (T3) treatments (GSE68867) [30]. This analysis identified a total of four genes exhibiting increased expression in T3-treated mouse livers, including the small leucine-rich repeat-containing protein Tsk, Fibronectin 1 (Fn1), Apolipoprotein M (Apom) and Secreted phosphoprotein 2 (Spp2). Fn1 and Spp2 are extracellular matrix proteins, whereas Apom is a component of plasma lipoproteins. Tsk is a highly conserved secreted protein that exhibits the highest mRNA expression in mouse liver compared to other tissues (Fig. 1b and Supplementary Fig. 1). We confirmed this expression profile by performing LacZ staining on tissues from mice harboring a Tsk gene trap allele and observed strong β-galactosidase activity in the liver, but not other tissues (Fig. 1c). Importantly, Tsk mRNA was detected primarily in hepatocytes, but not in non-parenchymal cells (NPC), suggesting that Tsk encodes a *bona fide* hepatokine (Fig. 1b). To determine whether mature TSK is released into circulation, we generated highly specific rabbit polyclonal antibodies against a C-terminal peptide of TSK. As shown in Fig. 1d, TSK protein was readily detectable in mouse plasma; the specific band was completely absent in plasma samples from Tsk knockout (KO) mice. We observed robust secretion of endogenous TSK protein by cultured primary hepatocytes isolated from wild type (WT), but not Tsk null mice (Fig. 1e).

TSK was previously described as a regulator of commissure formation though its expression in the brain was relatively low compared to the liver [31-33]. Its role in metabolic signaling and energy balance remained unknown. To determine whether hepatic Tsk expression and plasma TSK levels are responsive to increased energy expenditure, we examined these parameters in mice treated with T3 or CL 316,243, a β3-selective adrenergic agonist, or subjected to cold exposure for 4 hrs. Similar to chronic treatments, a single dose of T3 injection resulted in robust induction of Tsk mRNA expression and elevated TSK levels in circulation (Fig. 1f). Remarkably, a single dose of CL 316,243 treatment and acute cold exposure also stimulated hepatic Tsk mRNA expression, resulting in higher plasma TSK levels. These results strongly suggest that TSK is a hepatokine that is tightly linked to the activation of thermogenesis and energy expenditure. We next examined whether increased circulating TSK may provide a negative feedback signal to restrict energy expenditure in mice. In support of this, we observed that chow-fed Tsk null mice exhibited significantly higher core body temperature than WT littermates under *ad lib* condition (Fig. 1g). This elevation of body temperature in KO mice persisted following overnight starvation. More

importantly, fasting-induced weight loss was higher by approximately 36% in mice lacking TSK than control (Fig. 1h), indicating that Tsk null mice are hypermetabolic and fail to suppress energy expenditure in response to food deprivation.

TSK deficiency protects mice from HFD-induced obesity and metabolic disorders

To determine whether TSK dysregulation may facilitate positive energy balance in obesity, we next examined hepatic Tsk expression in diet-induced and genetic obesity in mice. Compared to lean control, Tsk mRNA expression was significantly elevated in high-fat diet (HFD)-fed and leptin receptor deficient (db/db) obese mouse livers (Fig. 2a and Supplementary Fig. 2). Hepatic Tsk mRNA levels positively correlated with weight gain in a cohort of wild type C57BL/6 mice following eight weeks of HFD feeding (Supplementary Fig. 2). Accordingly, plasma TSK levels were markedly elevated in HFD-fed and db/db mice (Fig. 2a), indicating that obesity is associated with aberrantly high TSK levels in circulation.

TSK deficient mice appeared normal by gross examination, weighed slightly less than littermate control, and did not exhibit significant changes in their metabolic parameters when fed standard rodent chow (Supplementary Fig. 3). Upon high-fat feeding, KO mice exhibited remarkable resistance to HFD-induced weight gain (Fig. 2b). WT mice gained an average of 66.3% body weight over a period of 14 weeks of high-fat feeding, whereas KO mice gained approximately 30.7%. Blood glucose levels were significantly lower in KO mice (Fig. 2c), whereas plasma total cholesterol and triglyceride (TAG) levels remained similar between two groups. Measurements of key circulating hormones indicated that, compared to control, plasma levels of insulin and leptin, but not FGF21, were markedly lower in Tsk null mice (Fig. 2d). Glucose tolerance test (GTT) and insulin tolerance test (ITT) indicated that Tsk null mice exhibited significantly improved insulin sensitivity and glucose tolerance (Fig. 2e).

Tsk null mice exhibited smaller eWAT, BAT and liver mass than control following HFD feeding (Fig. 2f and Supplementary Fig. 4a). As expected, brown fat from HFD-fed WT mice appeared pale in color as a result of whitening of brown adipocytes. In striking contrast, brown fat from Tsk null mice remained dark red and appeared similar to brown fat obtained from cold-exposed mice (Fig. 2g). Histological analysis revealed that brown adipocytes in interscapular BAT from HFD-fed KO mice had reduced fat content and contained smaller lipid droplets (Fig. 2h). Epididymal WAT (eWAT) from Tsk KO mice contained smaller adipocytes and fewer crown-like structures, suggesting that obesity-associated adipose tissue inflammation is attenuated by TSK deficiency. In support of this, mRNA expression of genes associated with macrophage and adipose inflammation was significantly lower in eWAT from Tsk KO mice (Supplementary Fig. 4b). Tsk null mice had improved hepatic steatosis as shown histologically and by the measurements of liver TAG content (Fig. 2h-i). To establish how TSK deficiency influences energy balance, we performed metabolic cage studies in WT and KO mice fed HFD for two weeks to minimize confounding factors of prolonged HFD feeding. Compared to control, Tsk null mice exhibited significantly elevated VO_2 and energy expenditure rate (EE) (Fig. 3a and Supplementary Fig. 5). In contrast, food intake and total locomotor activity appeared comparable in two groups. These results strongly suggest that TSK deficiency may abrogate

a negative feedback brake on whole body energy expenditure, resulting in resistance to diet-induced obesity.

TSK deficiency promotes adipose thermogenesis and energy expenditure

Brown fat thermogenesis is an important component of energy expenditure that contributes to defense against cold and obesity. We next examined whether Tsk inactivation results in stimulation of brown fat thermogenesis. Microarray analysis of brown fat gene expression identified a cluster of 202 genes that exhibited over 1.4-fold increase in Tsk KO mice (Fig. 3b). Gene ontology analysis indicated that this cluster was highly enriched for pathways involved in mitochondrion, lipid metabolism, nucleotide-binding and oxidoreductase. qPCR analysis confirmed that mRNA expression of key thermogenic markers, including Deiodinase 2 (Dio2) and Ucp1, was significantly higher in BAT from chow-fed Tsk null mice (Fig. 3c). UCP1 protein levels were also higher as a result of TSK deficiency (Fig. 3d). Remarkably, phosphorylation of hormone-sensitive lipase (HSL) and Protein Kinase A (PKA) substrates was markedly enhanced in brown fat obtained from Tsk KO mice. These results demonstrate that TSK deficiency augments adrenergic action and thermogenic stimulation in brown fat. Measurement of norepinephrine (NE) concentrations revealed that BAT, but not eWAT, exhibited significantly elevated NE levels as a result of TSK deficiency (Fig. 3e). In contrast, plasma NE levels were comparable between two groups, suggesting that TSK deficiency may enhance sympathetic outflow to brown fat to promote thermogenesis. Consistently, brown fat from HFD-fed Tsk null exhibited increased PKA substrate phosphorylation and UCP1 protein expression, characteristics of enhanced adrenergic activation (Fig. 3f). PKA substrate phosphorylation was also enhanced in inguinal WAT (iWAT) from HFD-fed Tsk null mice compared to control. DIO2 is responsible for the local activation of thyroid hormone, which acts in concert with adrenergic signaling to stimulate thermogenesis [34]. We found that BAT from Tsk KO mice had slightly but significantly increased T3 levels (Fig. 3g).

The studies above illustrated that TSK serves an important role in energy balance and metabolic physiology. However, whole body TSK deficiency may elicit unforeseen effects on developmental programs. In addition, it remains unknown whether the liver provides a major source of plasma TSK in metabolic regulation. To address these, we employed a recently developed CRISPR/Cas9 method to knock out Tsk in the liver in adult mice [35]. We generated a recombinant adenovirus-associated virus (AAV) expressing a pair of guide RNAs targeting the coding region of Tsk (gTsk). Tail vein injection of AAV-gTsk in Cas9 transgenic mice resulted in efficient deletion of Tsk in the liver and marked reduction of TSK in circulation (Fig. 4a-b), illustrating the hepatic origin of circulating TSK. We subjected mice transduced with AAV-GFP and AAV-gTsk to HFD feeding and analyzed their metabolic parameters. Compared to control, AAV-gTsk group tended to gain less body weight and had lower blood glucose, yet the data did not reach statistical significance (Fig. 4c). In contrast, AAV-gTsk mice had significantly lower plasma insulin concentrations, improved insulin sensitivity (Fig. 4d), and reduced lipid content in brown adipocytes (Fig. 4e). Immunoblotting analysis indicated that hepatic Tsk inactivation resulted in increased TH and UCP1 levels and enhanced adrenergic signaling (Fig. 4f), reminiscent of the

observations in whole body Tsk deficiency. These results support the notion that TSK of hepatic origin regulates adipose and systemic metabolism in adult mice.

TSK is a negative regulator of sympathetic innervation in brown fat

Adipose tissue is densely innervated by sympathetic nerve fibers that control adipocyte lipolysis and thermogenesis [36-38]. Adrenergic stimulation as a result of sympathetic outflow provides a major catabolic signal for adipose tissue that balances fat storage and utilization [12]. Low sympathetic activities and defective adrenergic signaling have been linked to reduced adipose tissue thermogenesis and brown fat whitening, leading to obesity and metabolic disorders [39,40]. The striking activation of adrenergic signaling in Tsk null adipose tissue raised the possibility that TSK may regulate sympathetic innervation of adipose tissue. In support of this, we observed elevated tyrosine hydroxylase (TH) protein levels in brown fat from Tsk KO mice (Fig. 3d). TH is a rate-limiting enzyme in catecholamine biosynthesis and serves as a marker for sympathetic nerve fibers. Notably, TH protein levels were markedly higher in Tsk KO BAT and iWAT than littermate control following HFD feeding (Fig. 3f). To directly visualize the effects of TSK deficiency on sympathetic innervation, we performed TH immunofluorescence staining on brown fat sections. Confocal microscopy revealed that the abundance of TH-positive punctae, which correspond to sympathetic fibers in cross section, was markedly increased in brown fat from Tsk KO mice (Fig. 5a-b). These results suggest that TSK may serve as a checkpoint for sympathetic innervation of adipose tissue.

We next performed denervation studies to further dissect the significance of sympathetic innervation in mediating the effects of TSK on brown fat thermogenesis. We transected the nerve that targets brown fat on one side and performed sham operation on the other side as control in the same animal. Similar to the above results, TH levels and PKA substrate phosphorylation were strongly elevated in Tsk KO brown fat on the sham-operated side (Fig. 5c). In contrast, sympathetic denervation completely abolished TH immunoreactivity and attenuated the increase of PKA substrate phosphorylation observed in KO brown fat. Histological analysis revealed that brown fat from Tsk null mice exhibited significant whitening following denervation (Fig. 5d). Further, the induction of Ucp1 and Dio2 by TSK deficiency was also reversed by denervation of brown fat (Fig. 5e).

We took an alternative approach to suppress sympathetic activity by thermoneutral housing. While Tsk KO mice were protected from HFD-induced brown fat whitening when housed at ambient room temperature, this protective effect was largely abolished when mice were housed at thermoneutral temperature (Fig. 5f). Accordingly, protection from diet-induced obesity in Tsk KO mice was also partially lost when HFD feeding was performed at thermoneutral temperature (Fig. 5g). These results suggest that enhanced sympathetic innervation likely serves as a critical mediator of the stimulatory effects of TSK deficiency on brown fat thermogenesis and energy expenditure. In support of this, recombinant TSK failed to exert significant effects on brown adipocyte differentiation and thermogenic activation (Supplementary Fig. 6). The expression of several neurotrophic factors, including Neuregulins and Nerve growth factor (NGF), was largely unaltered by TSK deficiency (Supplementary Fig. 7). In addition, recombinant TSK did not appear to affect NGF-induced

differentiation and neurite outgrowth in PC-12 cells, a commonly used cell culture model for sympathetic neurons. To search for cellular targets of TSK action, we generated a fusion protein between TSK and secreted alkaline phosphatase (SEAP) and performed hormone binding assay on frozen tissue sections. Both SEAP and TSK-SEAP exhibited similar background binding to heart, lung and the liver (Fig. 5h). In contrast, strong binding of TSK-SEAP, but not SEAP, was observed on brown fat sections. Our results support a model where TSK acts on one or more unique cellular targets in brown fat to modulate sympathetic innervation.

Discussion

In this study, we identified TSK as a liver-derived endocrine hormone that gates energy expenditure by acting as a checkpoint for adipose sympathetic innervation and adrenergic signaling (Fig. 6). Several lines of evidence support the notion that TSK serves as a feedback hormonal signal that attenuates energy expenditure. Hepatic Tsk expression and its plasma levels were strongly induced by stimuli that increase thermogenesis and energy expenditure, such as T3, adrenergic agonist and cold exposure. Mice lacking TSK exhibited elevated core body temperature and were unable to adequately suppress energy expenditure during starvation, leading to greater body weight loss. Tsk null mice were strongly resistant to diet-induced obesity, insulin resistance and hepatic steatosis as a result of enhanced sympathetic activation and brown fat thermogenesis. In fact, TSK deficiency increased sympathetic innervation and nearly completely blocked HFD-induced whitening of brown fat. Together, these results support a critical role of TSK as a hepatokine in the regulation of adipose and systemic energy metabolism.

The metabolic effects of TSK inactivation are in striking contrast to leptin deficiency; the latter results in diminished sympathetic tone, thermogenesis and severe obesity in mice and humans. As leptin serves as a fat-derived hormone that senses nutrient storage and excess, TSK appears to be highly responsive to thermogenesis and energy expenditure. We propose that a distributed endocrine signaling network involving multiple peripheral tissues and cell types acts together to ensure whole body energy and nutrient homeostasis. The remarkable dichotomy of leptin and TSK action on energy balance raises the possibility that these two feedback pathways may converge at certain yet-to-be-defined biochemical and cellular targets in the body to drive the downstream metabolic effects. Whether TSK deficiency and/or polymorphisms in humans confer protection against weight gain and metabolic disorders remains an intriguing possibility for future exploration.

The sympathetic nervous system provides a powerful neural signal that controls adipose tissue fuel mobilization and thermogenesis. Recent studies using three-dimensional imaging techniques revealed highly organized patterns and plasticity of sympathetic innervation in adipose tissue [41-43]. TSK deficiency greatly increased TH-positive fiber density in brown fat, suggesting that TSK signaling may serve an inhibitory role in adipose sympathetic innervation during development and postnatal growth. Recent work identified a unique population of adipose macrophage responsible for uptake and catabolism of catecholamines [44,45]. However, mRNA expression of Monoamine oxidase A, an enzyme responsible for catecholamine catabolism, appeared largely unaltered in TSK deficient BAT (data not

shown). These observations suggest that TSK modulates adipose tissue adrenergic signaling and thermogenesis primarily through its effects on sympathetic innervation. We observed TSK binding in brown fat; however, the identity of cellular target for TSK and its receptor remain currently unknown. Previous studies have demonstrated that TSK suppresses neurite outgrowth in cultured neurons [31]. It is possible that local enrichment of TSK via binding to brown fat tissue may attenuate sympathetic nerve fiber outgrowth and/or branching. Alternatively, retrograde TSK signaling in postganglionic sympathetic neurons may suppress TH expression and catecholamine synthesis. Our current study cannot rule out the possibility that TSK may act on the central nervous system to regulate sympathetic innervation and outflow. Nonetheless, our work delineates a negative feedback arm of energy expenditure that may serve as a target for therapeutic intervention of metabolic disease.

Methods

Mice.

All animal studies were performed following procedures approved by the Institutional Animal Care and Use Committee at the University of Michigan. Unless otherwise stated, mice used in this study were male C57BL/6 mice maintained under 12/12 h light/dark cycles with free access to food and water. To induce obesity, mice were fed standard chow (Teklad 5001) or a high-fat diet containing 60% of calories from fat (D12492, Research Diets) starting at 10-12 weeks of age. Tsk null mice were generated and maintained in C57BL/6 background as previously described [32]. The Cas9 transgenic mice were purchased from Jackson Laboratory (JAX #024858). Tsk inactivation in adult mice was performed using a CRISPR/Cas9 method previously described [35]. Briefly, 3-month-old Cas9 mice were injected with recombinant adenovirus-associated virus (AAV) expressing two sgRNAs (sgRNA1: *GGTTAAGAGTGTTCCAGGAG* and sgRNA2: *GAGATCCAGGCCAGCCAG-TG*) targeting Tsk (http://crispr.mit.edu/)[46]. For AAV transduction, we injected approximately 1×10^{11} genome copies of AAV vectors per mouse via tail vain.

Metabolic cage measurements were performed in littermate control and Tsk null male mice at the University of Michigan Animal Phenotyping Core, as previously described [23,35]. Energy expenditure, O_2 consumption, total locomotor activity and food intake were measured using the Comprehensive Lab Animal Monitoring System (CLAMS, Columbus Instruments). Fat and lean mass was measured using an NMR-based analyzer (Minispec IF90II, Bruker Optics). For cold experiment, 3-month-old mice were individually housed in pre-chilled cages at 4℃ with free access to food and water for 4 hrs. For thermoneutral housing experiments, mice were maintained at a temperature-controlled chamber at 30℃.

BAT denervation.

BAT denervation surgery was performed on WT and Tsk KO mice at 3 months of age. Mice were anesthetized with isoflurane and shaved of hair on nape regions. A lateral incision was made below shoulder blades, and intrascapular fat pads were retracted cranially over the head to expose five branches of intercostal sympathetic nerves subserving the left- and right-side BAT fat pad. For unilateral denervation, the left branch was severed between the root and the BAT, while the right branch was left intact. The intrascapular fat pad was then

returned to its original position and secured in place to the surrounding thoracic tissue and muscle with absorbable 6.0 VICRIL suture. Tissues were harvested and analyzed 14 days following denervation.

Cell culture.

Primary brown adipocytes were immortalized and differentiated in culture as previously described [47]. Briefly, confluent cells were incubated with induction medium (DMEM containing 10% FBS, 0.5 μM isobutylmethylxanthine (IBMX), 125 μM indomethacin, 1 μM dexamethasone, 1 nM triiodothyronine (T3), and 20 nM insulin). After 48 h, the medium was replaced with maintenance medium (DMEM supplemented with 10% FBS, 1 nM T3, and 20 nM insulin). For TSK treatments, recombinant human TSK protein (3940-TS; R&D Systems) was added to the induction medium at different concentrations. PC-12 cells were cultured in RPMI 1630 medium containing 10% horse serum and 5% FBS. For PC-12 cell differentiation, 40%-60% confluent cultures were exposed to RPMI 1640 containing 2% horse serum, 1% FBS and 100 ng/ml NGF (B5025, envigo). Fresh differentiation medium was added every two days until day 6.

Gene expression and immunoblotting analyses.

Total adipose tissue RNA was extracted using a commercial kit (12183025, Invitrogen). Total RNA from other tissues was extracted using TRIzol (Invitrogen). Gene expression was analyzed by qPCR using the primers shown in the Supplementary Table 3. For microarray study of brown fat gene expression, total brown fat RNA from chow-fed WT and Tsk KO mice was analyzed using Affymetrix Mouse Gene ST 2.1 array strips. Sample processing and data analyses were performed according to the manufacturer's instructions.

For immunoblotting, total lysates were prepared in a lysis buffer containing 50 mM Tris (pH=7.5), 150 mM NaCl, 5 mM NaF, 25 mM β-glycerol phosphate, 1 mM dithiothreitol (DTT), and freshly added protease inhibitors. Protein lysates were separated by SDS-PAGE gels, transferred to polyvinylidene difluoride membrane, and immunoblotting with the following primary antibody. Rabbit polyclonal antibody to TSK was generated with mouse Tsk peptide (CRRLVREGAYHRQPGSSPK, Tsk amino acids 317-335) followed by affinity purification. Antibody against phospho-PKA substrate (catalog 9624), phospho-HSL (Ser660) (catalog 4126), and HSL (catalog 4107) were purchased from Cell Signaling Technology. Antibody against phospho-Perilipin (Ser497) (catalog 4855) and Perilipin (catalog 4854) were purchased from Vala Sciences. Antibody against UCP1 (UCP11-A) was purchased from Alpha Diagnosis. Antibody against Tubulin (T6199) was purchased from Sigma-Aldrich. Antibody against HSP90 (sc-7947) was purchased from Santa Cruz. Antibody against tyrosine hydroxylase (ab112) was purchased from Abcam.

β-gal staining.

To determine Tsk mRNA expression profile in mice, β-gal staining was performed on tissues from WT and Tsk heterozygous mice. Briefly, tissues were dissected, cut into small pieces and fixed with cold formalin for 30 min. The tissues were washed three times with PBS and subsequently incubated with 1 mg/ml X-gal for 30 min.

Plasma and liver triglyceride measurements.

Plasma concentrations of total cholesterol were measured using kits from Stanbio Laboratory (1010-430). Plasma concentrations of triglyceride were measured using kit from Sigma (Tr0100). Plasma concentrations of insulin and leptin were measured using commercial ELISA kits from Crystal Chem (90080 and 90030, respectively). Plasma FGF21 level was measured using mFGF21 ELISA kit (MF2100, R&D Systems). Liver lipids were extracted and measured as previously described [48]. Briefly, 100-150 mg liver tissue was homogenized in 2 ml lysis buffer containing 50 mM Tris (pH=7.5), 5 mM EDTA, 300 mM Mannitol and 1 mM PMSF. Homogenates (200 μl) were mixed with 5 μl KOH (10 M) and extracted with 800 μl chloroform/Methanol (2:1). The organic phase was mixed with equal volumes of Chloroform/Methanol/H_2O (3:48:47) followed by rigorous vortex and centrifuged at 10,000g for 10 min. The bottom layer was transferred to a new tube and dried in fume hood overnight. The resulting lipids were resuspended with 50 μl triglyceride resuspension buffer (Butanol/[Triton-X114/Methanol (2:1)](3:2)). Triglyceride content was measured using kit from Sigma (337-B) and normalized to the liver weight.

GTT and ITT.

Glucose and insulin tolerance test (GTT and ITT) were performed as previously described [23]. For GTT, mice were fasted for overnight (16h), and injected intraperitoneally with a glucose solution at 1.0 g per kg body weight. Blood glucose concentrations were measured before and 20, 45, 90 and 120 min after glucose injection. For ITT, mice were fasted for 4 hrs and then injected intraperitoneally with insulin at 0.7 U per kg body weight. Blood glucose concentrations were measured before and 20, 45, 90 and 120 min after insulin injection.

Histology.

Liver and WAT sections were embedded in paraffin and then stained with H&E. For immunofluorescence, Brown fat tissues were fixed in 4% paraformaldehyde for overnight at 4℃ and then incubated with 30% sucrose for 48 h before embedding in the OCT compound. Samples were blocked with 20% normal horse serum and incubated with the antibody against mouse tyrosine hydroxylase for overnight at 4℃, followed by incubation with a fluorophore-conjugated secondary antibody (Thermo Fisher Scientific) for 1 hr. The sections were mounted with DAPI-containing mounting medium (VECTASHIELD) for fluorescent microscopy.

Catecholamine measurements.

Plasma and tissue norepinephrine levels were measured using reverse-phase UltiMate 3000 HPLC system with electrochemical detection (Thermo Fisher). Briefly, individual BAT and eWAT samples were homogenized using perchloric acid (0.2 M) supplemented with ascorbic acid (1 mg/ml) and dihydroxybenzylamide (DHBA) as an internal standard. Active alumina was used to extract catecholamines from the homogenates followed by elution with 200 μl of perchloric acid with ascorbic acid.

TSK binding assay.

Hormone binding assay was performed as previously described [49,50]. Hepa-1 cells were transduced with retrovirus expressing SEAP or TSK-SEAP. Conditioned media from Hepa-1 cells were harvested and used in binding assay. Briefly, frozen tissue sections were incubated with SEAP or TSK-SEAP CM for 45 min at room temperature. Slides were washed with PBS containing 0.1% Tween-20 and fixed in a solution containing 20 mM HEPES (PH 7.4), 60% acetone and 3% formaldehyde. After inactivating endogenous alkaline phosphatase at 65℃ for 30 min, the enzymatic activity derived from the fusion protein was detected using NBT/BCIP substrate.

Statistics and reproducibility.

Two-tailed Student's t test was used to analyze the differences between two groups. Two-way ANOVA with multiple comparisons was used for statistical analysis of GTT, ITT and body weight studies. A P value of less than 0.05 was considered statistically significant. Statistical methods and corresponding P values for data in each panel were shown in the figure legends. All mouse experiments were independently replicated for at least twice. The cell culture experiments were performed in triplicates and repeated at least three times. We did not exclude any data points or mice unless a technical issue or human error occurs.

Reporting summary.

Further information on research design is available in the Nature Research Reporting Summary.

Data availability.

The microarray dataset described in the paper has been deposited into Gene Expression Omnibus database (https://www.ncbi.nlm.nih.gov/geo/) with accession number GSE114361. All other data are available from the corresponding author on reasonable request.

Supplementary Material

Refer to Web version on PubMed Central for supplementary material.

Acknowledgments

This work was supported by NIH grants (DK102456 and AG055379 to J.D.L.; DK114220 to L.R.), the Michigan Diabetes Research Center (DK020572), and the Michigan Nutrition and Obesity Center (DK089503).

REFERENCES

1. Pedersen BK & Febbraio MA Muscles, exercise and obesity: skeletal muscle as a secretory organ. Nat Rev Endocrinol 8, 457–465, doi:10.1038/nrendo.2012.49 (2012). [PubMed: 22473333]
2. Potthoff MJ, Kliewer SA & Mangelsdorf DJ Endocrine fibroblast growth factors 15/19 and 21: from feast to famine. Genes Dev 26, 312–324, doi:10.1101/gad.184788.111 (2012). [PubMed: 22302876]
3. Trujillo ME & Scherer PE Adipose tissue-derived factors: impact on health and disease. Endocr Rev 27, 762–778, doi:10.1210/er.2006-0033 (2006). [PubMed: 17056740]
4. Waki H & Tontonoz P Endocrine functions of adipose tissue. Annu Rev Pathol 2, 31–56, doi: 10.1146/annurev.pathol.2.010506.091859 (2007). [PubMed: 18039092]

5. Flier JS & Maratos-Flier E Leptin's Physiologic Role: Does the Emperor of Energy Balance Have No Clothes? Cell Metab 26, 24–26, doi:10.1016/j.cmet.2017.05.013 (2017). [PubMed: 28648981]
6. Friedman J 20 years of leptin: leptin at 20: an overview. J Endocrinol 223, T1–8, doi:10.1530/JOE-14-0405 (2014). [PubMed: 25121999]
7. Staiger H, Keuper M, Berti L, Hrabe de Angelis M & Haring HU Fibroblast Growth Factor 21-Metabolic Role in Mice and Men. Endocr Rev 38, 468–488, doi:10.1210/er.2017-00016 (2017). [PubMed: 28938407]
8. Stefan N & Haring HU The role of hepatokines in metabolism. Nat Rev Endocrinol 9, 144–152, doi:10.1038/nrendo.2012.258 (2013). [PubMed: 23337953]
9. Yanagi S, Sato T, Kangawa K & Nakazato M The Homeostatic Force of Ghrelin. Cell Metab 27, 786–804, doi:10.1016/j.cmet.2018.02.008 (2018). [PubMed: 29576534]
10. Crewe C, An YA & Scherer PE The ominous triad of adipose tissue dysfunction: inflammation, fibrosis, and impaired angiogenesis. J Clin Invest 127, 74–82, doi:10.1172/JCI88883 (2017). [PubMed: 28045400]
11. Martinez-Santibanez G & Lumeng CN Macrophages and the regulation of adipose tissue remodeling. Annu Rev Nutr 34, 57–76, doi:10.1146/annurev-nutr-071812-161113 (2014). [PubMed: 24850386]
12. Reilly SM & Saltiel AR Adapting to obesity with adipose tissue inflammation. Nat Rev Endocrinol 13, 633–643, doi:10.1038/nrendo.2017.90 (2017). [PubMed: 28799554]
13. Rosen ED & Spiegelman BM What we talk about when we talk about fat. Cell 156, 20–44, doi:10.1016/j.cell.2013.12.012 (2014). [PubMed: 24439368]
14. Cannon B & Nedergaard J Brown adipose tissue: function and physiological significance. Physiol Rev 84, 277–359, doi:10.1152/physrev.00015.2003 (2004). [PubMed: 14715917]
15. Harms M & Seale P Brown and beige fat: development, function and therapeutic potential. Nat Med 19, 1252–1263, doi:10.1038/nm.3361 (2013). [PubMed: 24100998]
16. Townsend KL & Tseng YH Brown fat fuel utilization and thermogenesis. Trends Endocrinol Metab 25, 168–177, doi:10.1016/j.tem.2013.12.004 (2014). [PubMed: 24389130]
17. Wu J, Cohen P & Spiegelman BM Adaptive thermogenesis in adipocytes: is beige the new brown? Genes Dev 27, 234–250, doi:10.1101/gad.211649.112 (2013). [PubMed: 23388824]
18. Ikeda K et al. UCP1-independent signaling involving SERCA2b-mediated calcium cycling regulates beige fat thermogenesis and systemic glucose homeostasis. Nat Med 23, 1454–1465, doi:10.1038/nm.4429 (2017). [PubMed: 29131158]
19. Ikeda K, Maretich P & Kajimura S The Common and Distinct Features of Brown and Beige Adipocytes. Trends Endocrinol Metab 29, 191–200, doi:10.1016/j.tem.2018.01.001 (2018). [PubMed: 29366777]
20. Kazak L et al. A creatine-driven substrate cycle enhances energy expenditure and thermogenesis in beige fat. Cell 163, 643–655, doi:10.1016/j.cell.2015.09.035 (2015). [PubMed: 26496606]
21. Chen Z et al. Nrg4 promotes fuel oxidation and a healthy adipokine profile to ameliorate diet-induced metabolic disorders. Mol Metab 6, 863–872, doi:10.1016/j.molmet.2017.03.016 (2017). [PubMed: 28752050]
22. Guo L et al. Hepatic neuregulin 4 signaling defines an endocrine checkpoint for steatosis-to-NASH progression. J Clin Invest, doi:10.1172/JCI96324 (2017).
23. Wang GX et al. The brown fat-enriched secreted factor Nrg4 preserves metabolic homeostasis through attenuation of hepatic lipogenesis. Nat Med 20, 1436–1443, doi:10.1038/nm.3713 (2014). [PubMed: 25401691]
24. Lowell BB et al. Development of obesity in transgenic mice after genetic ablation of brown adipose tissue. Nature 366, 740–742, doi:10.1038/366740a0 (1993). [PubMed: 8264795]
25. Yoneshiro T et al. Recruited brown adipose tissue as an antiobesity agent in humans. The Journal of clinical investigation 123, 3404–3408, doi:10.1172/JCI67803 (2013). [PubMed: 23867622]
26. Bartelt A et al. Brown adipose tissue activity controls triglyceride clearance. Nature medicine 17, 200–205, doi:10.1038/nm.2297 (2011).

27. van der Lans AA et al. Cold acclimation recruits human brown fat and increases nonshivering thermogenesis. The Journal of clinical investigation 123, 3395–3403, doi:10.1172/JCI68993 (2013). [PubMed: 23867626]
28. Cho KW, Zhou Y, Sheng L & Rui L Lipocalin-13 regulates glucose metabolism by both insulin-dependent and insulin-independent mechanisms. Mol Cell Biol 31, 450–457, doi:10.1128/MCB.00459-10 (2011). [PubMed: 21135134]
29. Meex RC et al. Fetuin B Is a Secreted Hepatocyte Factor Linking Steatosis to Impaired Glucose Metabolism. Cell Metab 22, 1078–1089, doi:10.1016/j.cmet.2015.09.023 (2015). [PubMed: 26603189]
30. Ohba K et al. Desensitization and Incomplete Recovery of Hepatic Target Genes After Chronic Thyroid Hormone Treatment and Withdrawal in Male Adult Mice. Endocrinology 157, 1660–1672, doi:10.1210/en.2015-1848 (2016). [PubMed: 26866609]
31. Hossain M et al. The combinatorial guidance activities of draxin and Tsukushi are essential for forebrain commissure formation. Dev Biol 374, 58–70, doi:10.1016/j.ydbio.2012.11.029 (2013). [PubMed: 23206892]
32. Ito A et al. Tsukushi is required for anterior commissure formation in mouse brain. Biochem Biophys Res Commun 402, 813–818, doi:10.1016/j.bbrc.2010.10.127 (2010). [PubMed: 21055390]
33. Ohta K et al. Tsukushi functions as an organizer inducer by inhibition of BMP activity in cooperation with chordin. Dev Cell 7, 347–358, doi:10.1016/j.devcel.2004.08.014 (2004). [PubMed: 15363410]
34. de Jesus LA et al. The type 2 iodothyronine deiodinase is essential for adaptive thermogenesis in brown adipose tissue. J Clin Invest 108, 1379–1385, doi:10.1172/JCI13803 (2001). [PubMed: 11696583]
35. Zhao XY et al. Long noncoding RNA licensing of obesity-linked hepatic lipogenesis and NAFLD pathogenesis. Nat Commun 9, 2986, doi:10.1038/s41467-018-05383-2 (2018). [PubMed: 30061575]
36. Bartness TJ, Liu Y, Shrestha YB & Ryu V Neural innervation of white adipose tissue and the control of lipolysis. Front Neuroendocrinol 35, 473–493, doi:10.1016/j.yfrne.2014.04.001 (2014). [PubMed: 24736043]
37. Morrison SF & Madden CJ Central nervous system regulation of brown adipose tissue. Compr Physiol 4, 1677–1713, doi:10.1002/cphy.c140013 (2014). [PubMed: 25428857]
38. Zeng W et al. Sympathetic neuro-adipose connections mediate leptin-driven lipolysis. Cell 163, 84–94, doi:10.1016/j.cell.2015.08.055 (2015). [PubMed: 26406372]
39. Bachman ES et al. betaAR signaling required for diet-induced thermogenesis and obesity resistance. Science 297, 843–845, doi:10.1126/science.1073160 (2002). [PubMed: 12161655]
40. Bray GA & York DA The MONA LISA hypothesis in the time of leptin. Recent Prog Horm Res 53, 95–117; discussion 117-118 (1998). [PubMed: 9769705]
41. Cao Y, Wang H, Wang Q, Han X & Zeng W Three-dimensional volume fluorescence-imaging of vascular plasticity in adipose tissues. Mol Metab, doi:10.1016/j.molmet.2018.06.004 (2018).
42. Chi J et al. Three-Dimensional Adipose Tissue Imaging Reveals Regional Variation in Beige Fat Biogenesis and PRDM16-Dependent Sympathetic Neurite Density. Cell Metab 27, 226–236 e223, doi:10.1016/j.cmet.2017.12.011 (2018). [PubMed: 29320703]
43. Jiang H, Ding X, Cao Y, Wang H & Zeng W Dense Intra-adipose Sympathetic Arborizations Are Essential for Cold-Induced Beiging of Mouse White Adipose Tissue. Cell Metab 26, 686–692 e683, doi:10.1016/j.cmet.2017.08.016 (2017). [PubMed: 28918935]
44. Camell CD et al. Inflammasome-driven catecholamine catabolism in macrophages blunts lipolysis during ageing. Nature 550, 119–123, doi:10.1038/nature24022 (2017). [PubMed: 28953873]
45. Pirzgalska RM et al. Sympathetic neuron-associated macrophages contribute to obesity by importing and metabolizing norepinephrine. Nat Med 23, 1309–1318, doi:10.1038/nm.4422 (2017). [PubMed: 29035364]
46. Ran FA et al. Genome engineering using the CRISPR-Cas9 system. Nature protocols 8, 2281–2308, doi:10.1038/nprot.2013.143 (2013). [PubMed: 24157548]

47. Zhao XY, Li S, Wang GX, Yu Q & Lin JD A long noncoding RNA transcriptional regulatory circuit drives thermogenic adipocyte differentiation. Molecular cell 55, 372–382, doi:10.1016/j.molcel.2014.06.004 (2014). [PubMed: 25002143]

48. Li S et al. Genome-wide coactivation analysis of PGC-1alpha identifies BAF60a as a regulator of hepatic lipid metabolism. Cell metabolism 8, 105–117, doi:10.1016/j.cmet.2008.06.013 (2008). [PubMed: 18680712]

49. Muller H, Dai G & Soares MJ Placental lactogen-I (PL-I) target tissues identified with an alkaline phosphatase-PL-I fusion protein. J Histochem Cytochem 46, 737–743, doi:10.1177/002215549804600606 (1998). [PubMed: 9603785]

50. Lin J & Linzer DI Induction of megakaryocyte differentiation by a novel pregnancy-specific hormone. The Journal of biological chemistry 274, 21485–21489 (1999). [PubMed: 10409714]

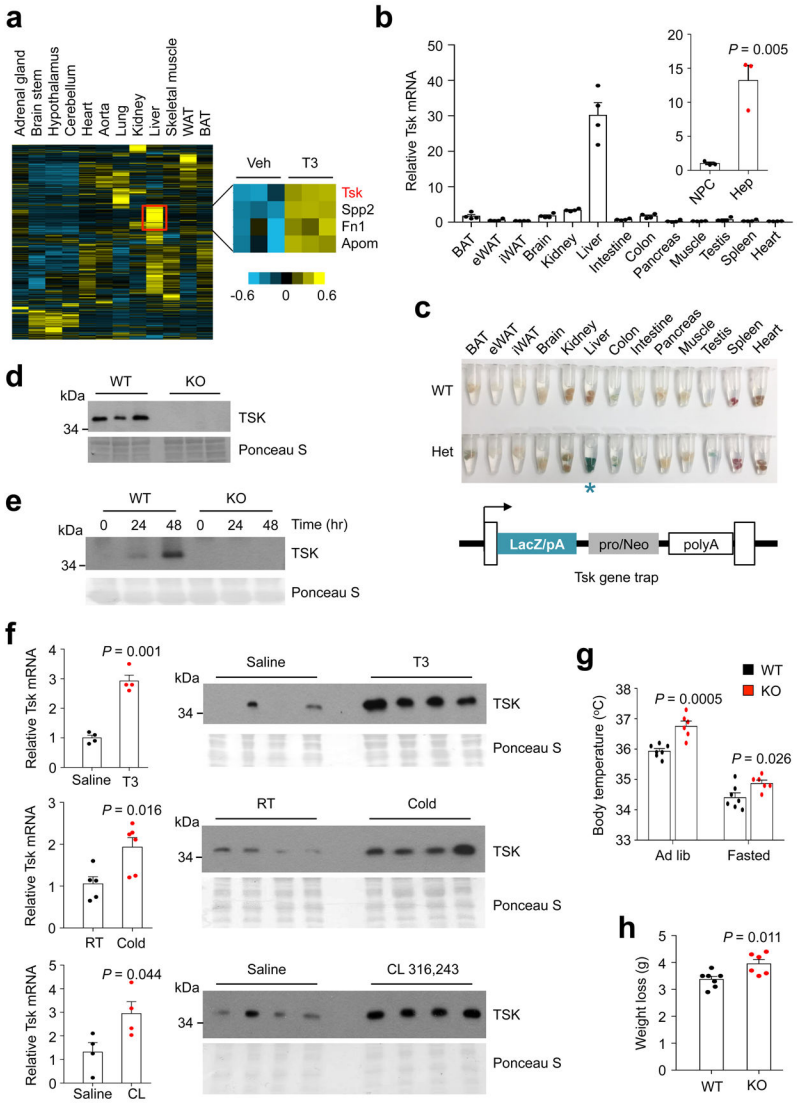

Fig. 1. TSK is a hepatokine responsive to increased energy expenditure.

(**a**) Heat map representation of secretome gene expression in chow-fed mouse tissues (left). The red box indicates a cluster of genes encoding liver-enriched secreted factors, four of which are induced by T3 treatment (right). (**b**) qPCR analysis of Tsk expression in mouse tissues (n=4) and in fractionated hepatocytes (Hep) and non-parenchymal cells (NPC) (n=3). (**c**) LacZ staining of tissues from mice containing a Tsk gene trap allele. Note the presence of strong β-galactosidase activity in the liver (blue asterisk). (**d**) Immunoblots of total plasma proteins from WT and Tsk KO mice. Ponceau S staining is shown as loading control. (**e**) TSK immunoblot of conditioned media collected from cultured WT and KO hepatocytes at indicated time points. (**f**) qPCR analysis of hepatic Tsk expression (left) and immunoblots of plasma (right) from mice treated with T3 (500 μg/kg) (Saline, n=4; T3, n=4), CL 316,243 (1 mg/kg) (Saline, n=4; CL, n=4), or cold exposure for 4 hrs(RT, n=5; Cold, n=6). (**g**) Rectal body temperature in WT (n=7) and Tsk KO (n=6) mice under *ad lib* condition and following 24 hrs of fasting. (**h**) Body weight loss in WT (n=7) and Tsk KO (n=6) mice following 24

hrs of food deprivation. Two-tailed unpaired Student's t test (**b, f, h**); two-way ANOVA (**g**); Data are mean ± SEM of biologically independent samples.

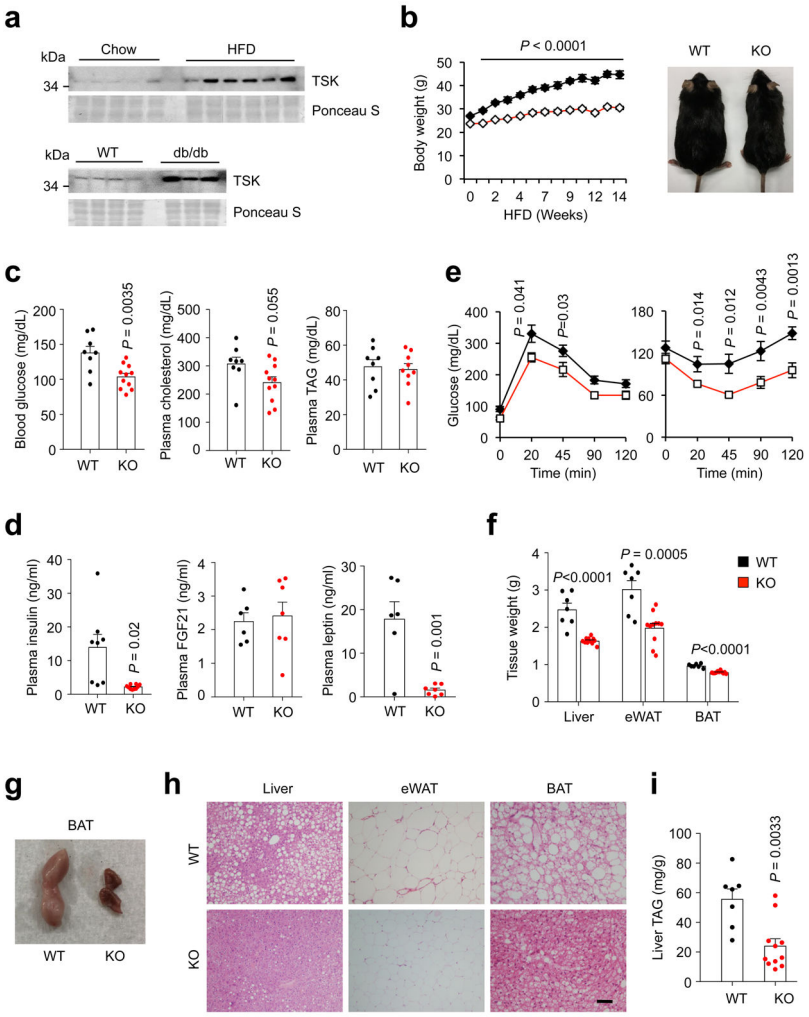

Fig. 2. TSK facilitates diet-induced obesity and brown fat whitening.

(**a**) Immunoblots of plasma from lean and obese mice. (**b**) Body weight of male WT (n=9) and Tsk KO (n=12) mice during HFD feeding. (**c**) Plasma glucose and lipid concentrations (WT, n=8; KO, n=10, except KO plasma TAG, n=9). (**d**) Plasma insulin (WT, n=8; KO, n=10), FGF21 and leptin (WT, n=6; KO, n=7) levels. (**e**) GTT and ITT in HFD-fed WT (n=9) and Tsk KO (n=12) mice. (**f**) Tissue weight of HFD-fed mice (WT, n=7; KO, n=11). (**g**) Morphology of brown fat from HFD-fed mice. (**h**) H&E staining of tissue sections (bar=100μm). (**i**) Liver TAG content (WT, n=7; KO, n=11). Two-tailed unpaired Student's t test (**c, d, f, i**); two-way ANOVA (**b**); Data are mean ± SEM of biologically independent samples.

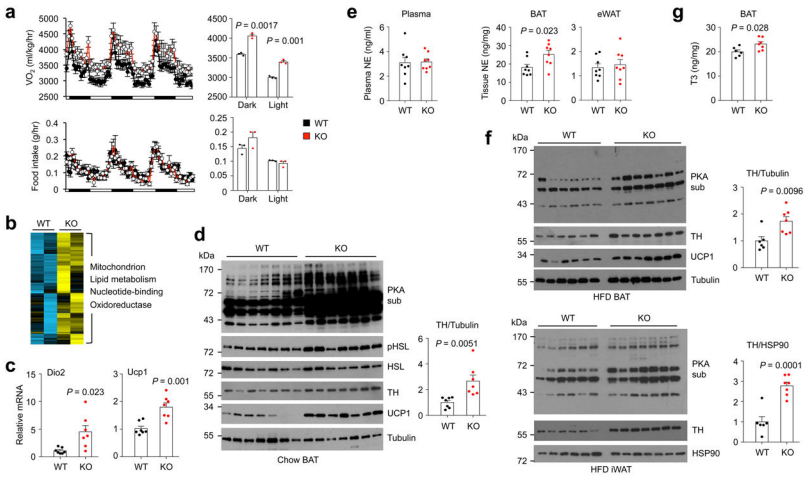

Fig. 3. TSK ablation relieves a brake on sympathetic action in adipose tissue.

(**a**) Oxygen consumption rate (top) and food intake (bottom) in male WT (n=8) and Tsk KO (n=8) mice following two weeks of high-fat feeding. Averaged oxygen consumption rate and food intake in dark and light phases are indicated on the right. (**b**) Heat map of a cluster of genes induced by >1.4-fold in brown fat from Tsk KO mice. Enriched pathways in this cluster are indicated. (**c**) qPCR analysis of Dio2 and Ucp1 mRNA expression in BAT (n=7). (**d**) Immunoblots of total brown fat lysates from chow-fed mice. Relative TH band intensity was quantified using Image J (right) (n=7). (**e**) Plasma and adipose tissue NE concentrations from WT (n=8) and Tsk KO (n=8) mice. (**f**) Immunoblots of total brown fat lysates from HFD-fed mice (WT, n=6; KO, n=7). (**g**) Brown fat T3 content from WT (n=6) and Tsk KO (n=7) mice. Two-tailed unpaired Student's t test (**a, c-g**); Data are mean ± SEM of biologically independent samples.

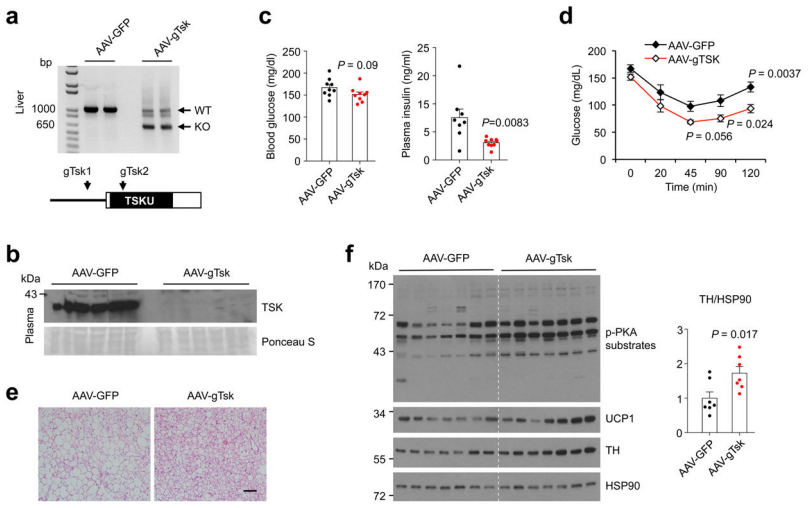

Fig. 4. Hepatic Tsk inactivation ameliorates HFD-induced insulin resistance.

(**a**) CRISPR/Cas9-mediated inactivation of Tsk in adult mice. Guide RNAs targeting Tsk are indicated. (**b**) Immunoblot of total plasma proteins from transduced mice. (**c**) Blood glucose and plasma insulin concentrations in mice transduced with AAV-GFP (n=8) or AAV-gTsk (n=9) after 16 weeks of HFD feeding. (**d**) Insulin tolerance test (n=9). (**e**) H&E staining of BAT sections. (**f**) Immunoblots of total brown fat lysates (n=7). Two-tailed unpaired Student's t test (**c, f**); two-way ANOVA (**d**); Data are mean ± SEM of biologically independent samples.

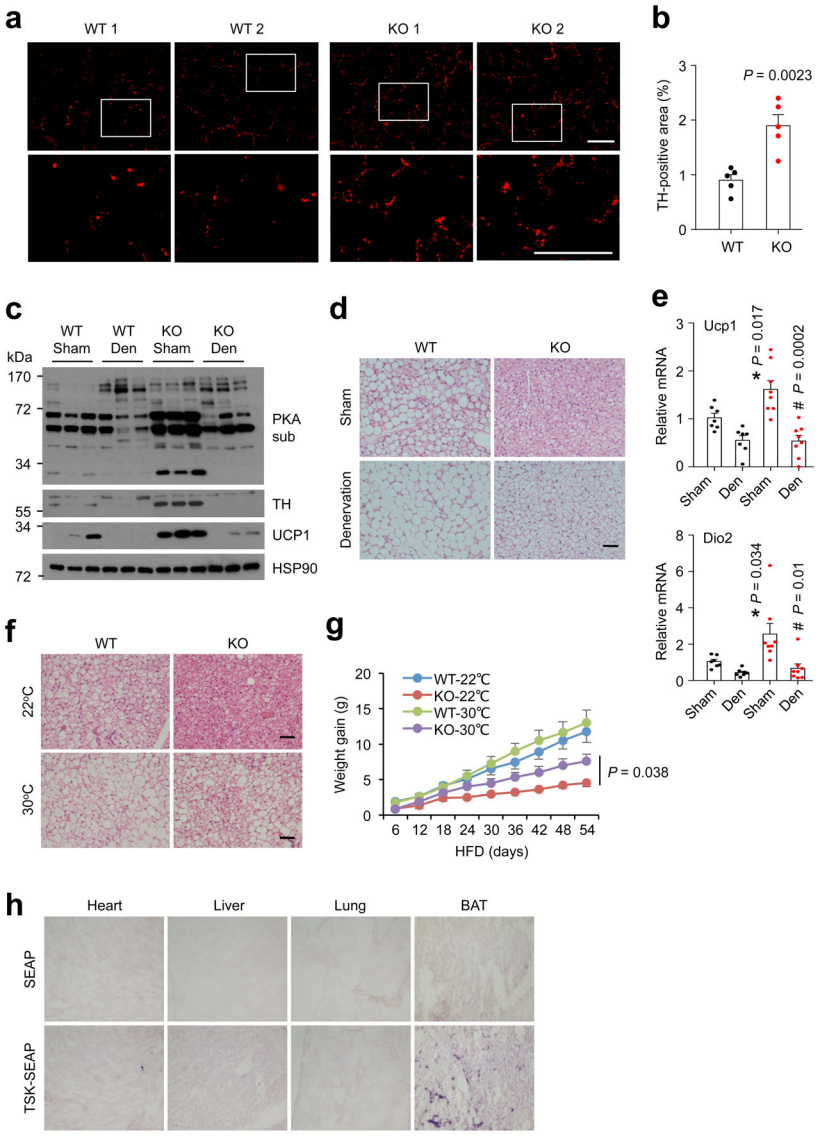

Fig. 5. TSK regulates brown fat thermogenesis through sympathetic innervation.

(**a**) TH immunofluorescence staining on frozen BAT sections from chow-fed mice (bar=50 μm). (**b**) Quantitation of TH-positive area on WT and KO mouse BAT sections (n=5). (**c**) Immunoblots of total lysates from sham or denervated (Den) brown fat from WT and Tsk KO mice. (**d**) H&E staining of sham and denervated brown fat (bar=100μm). (**e**) qPCR analysis of Dio2 and Ucp1 mRNA expression in sham and denervated brown fat from WT (n=7) and Tsk KO (n=8) mice, WT sham vs. KO sham (*); KO sham vs. KO den (#). (**f**) H&E staining of brown fat from mice housed at 22°C and 30°C (bar=100μm). (**g**) HFD-induced weight gain in WT and Tsk KO mice housed at 22°C (WT, n=6; KO, n=4) and 30°C (WT, n=7; KO, n=5). (**h**) Hormone binding assay. Two-tailed unpaired Student's t test (**b, e, g**); Data are mean ± SEM of biologically independent samples.

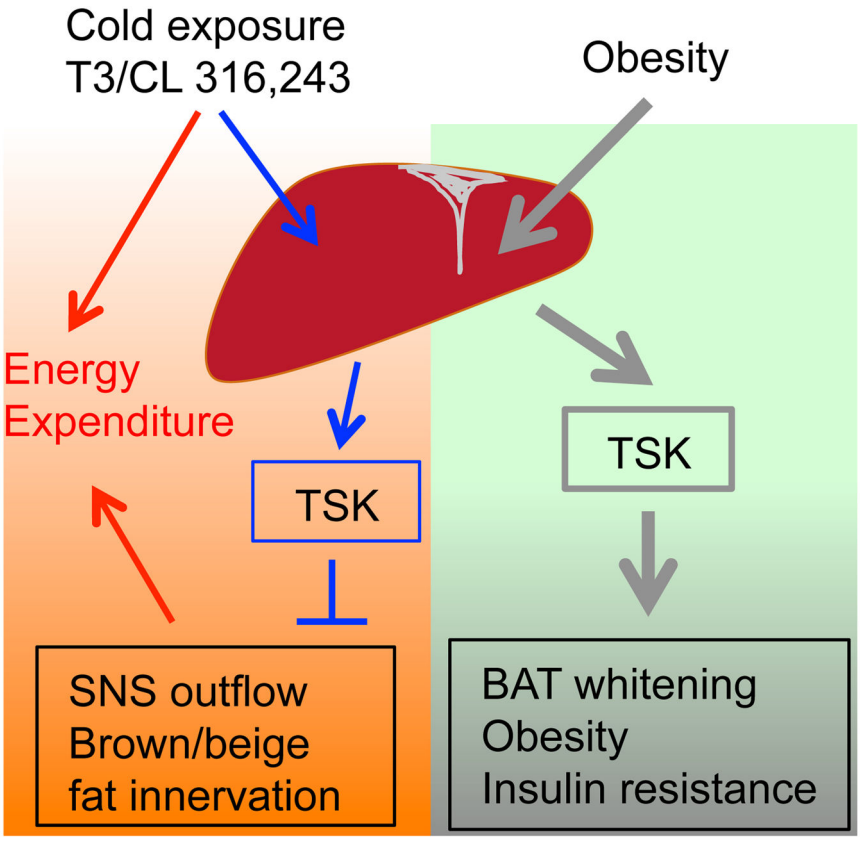

Fig. 6. Role of TSK as a hepatokine checkpoint for thermogenesis and energy balance.

TSK is induced in response to increased energy expenditure, providing a negative feedback mechanism to suppress sympathetic activation of thermogenesis. Excess TSK in obesity promotes brown fat whitening, HFD-induced weight gain and metabolic disorders.